Optical singularity assisted method for accurate parameter detection of step-shaped nanostructure in coherent Fourier scatterometry

Dou, Xiujie; Min, Changjun; Zhang, Yuquan; Pereira, S. F.; Yuan, Xiaocong

DOI
10.1364/OE.462045

Publication date
2022

Document Version
Final published version

Published in
Optics Express

Citation (APA)
Dou, X., Min, C., Zhang, Y., Pereira, S. F., & Yuan, X. (2022). Optical singularity assisted method for accurate parameter detection of step-shaped nanostructure in coherent Fourier scatterometry. *Optics Express*, *30*(16), 29287-29294. https://doi.org/10.1364/OE.462045

Important note
To cite this publication, please use the final published version (if applicable).
Please check the document version above.

Research Article | Vol. 30, No. 16 / 1 Aug 2022 / Optics Express 29287
Optics EXPRESS

Optical singularity assisted method for accurate parameter detection of step-shaped nanostructure in coherent Fourier scatterometry

XIUJIE DOU,[1,2] CHANGJUN MIN,[1,3] YUQUAN ZHANG,[1] S. F. PEREIRA,[2] AND XIAOCONG YUAN[1,4]

[1]*Nanophotonics Research Centre, Shenzhen Key Laboratory of Micro-Scale Optical Information Technology & Institute of Microscale Optoelectronics, Shenzhen University, Shenzhen 518060, China*
[2]*Optics Research Group, Department of Imaging Physics, Faculty of Applied Sciences, Delft University of Technology, Lorentzweg 1,2628 CJ Delft, The Netherlands*
[3]*cjmin@szu.edu.cn*
[4]*xcyuan@szu.edu.cn*

Abstract: Accurate determination of the physical parameters of nanostructures from optical far-field scattering is an important and challenging topic in the semiconductor industry. Here, we propose a novel metrology method to determine simultaneously the height and side-wall angle of a step-shaped silicon nanostructure. By employing an optical singular beam into a typical coherent Fourier scatterometry system, both parameters can be retrieved through analyzing the intensity profile of the far-field scattering pattern. The use of singular beam is shown to be sensitive to slight changes of the parameters of the step. By changing the relative direction between the singularity and structure, the height and side-wall angle can both be retrieved with high precision. This new method is robust, simple, and can provide valuable means for micro-and-nano- metrologies.

1. Introduction

With the continuously reduction of the dimensions of semiconductor devices, there has been a strong demand for a simple, robust, non-invasive, and far-field optical detection technique that is sensitive to nanoscale dimensions. This demand is mainly driven by the requirements of the production quality control, in-line process control and production equipment in the semiconductor industry. Several near-field microscopy systems [1–5] such as atomic force microscopy and scanning electron microscopy, can provide extremely high resolution. However, they are not suitable for industrial environment since they operate mostly off-line, they are expensive, have low throughput and may be invasive. In principle, optical methods are good candidates to overcome those difficulties. Optical scatterometry [6,7], which uses the far-field optical scattering to retrieve the geometrical features of a structure, is a non-invasive in-situ detection method, of which Fourier Scatterometry (FS) occupies a place in it. In FS, the light that is scattered from the structure at different angles is recorded and analyzed at the Fourier plane in one shot [8–10]. Coherent Fourier scatterometry (CFS) uses a coherent focused beam to illuminate the structure [11]. The use of coherent illumination makes CFS quite competitive and even superior to the incoherent counterpart. CFS has been successfully applied to detect the shape parameters of grating structures as well as for nano-particles and contamination detection [12–15].

Spatially modulated structure light, which refers to a light beam with specially designed intensity, phase, or polarization distribution patterns [16–18], has drawn extensive attention of researchers because of its novel characteristics in many fields. Structured light beams with optical singularity, termed as singular beam [19–21], has potential for a lot of applications. The singularities often refer to the discontinuities in phase or polarization in the light field, and the

#462045 https://doi.org/10.1364/OE.462045
Journal © 2022 Received 22 Apr 2022; revised 2 Jul 2022; accepted 15 Jul 2022; published 26 Jul 2022

Optics EXPRESS

optical field intensity usually has a sharp decrease near the singularity. It has been shown that the dark singularity can be extremely sensitive to detect slight changes in the field due to its interaction with (nano)objects [22–28]. Such property of the singular beam has been verified to be feasible in precise measurement of nanostructures [24].

In this paper, we employ a singular beam on a CFS scheme to determine both the height and side-wall angle (SWA) of a step-shaped silicon nanostructure simultaneously. A numerical 3-dimensional rigorous model is built, and the scattered far-field intensity is obtained for further analysis. Due to the high sensitivity driven by the singularity line of the beam, we propose a bi-modal detection to decouple the changes of each of the parameters that is observed in the far field data. The numerical results demonstrate that the proposed approach can distinguish tiny differences in these two parameters. As an effective and robust method, this work could provide a good complement to the CFS technique for finer measurements of nanostructures.

2. Method

In conventional CFSs, the nanostructure sample is illuminated by a coherent focused beam with a truncated Gaussian spatial profile, and is then further investigated via a raster-scanning of the structure. Here, we introduce a (1,0) mode Hermite-Gaussian (HG_{10}) singular beam (with a line singularity in the center) into the conventional CFS to improve the detection sensitivity. Most nanostructures used to characterize the quality of nano fabrication have local steep walls and ridges of different widths. For simplicity, here, the studied structure is selected as a step-shaped silicon structure with height and SWA within the x-z plane, and invariant with respect to the y-axis. The schematics of the entire system is depicted in Fig. 1(a). To get the desired HG_{10} beam, the incident collimated beam (λ=633 nm) is firstly transformed to a radially polarized beam (RPB) by passing through a linear polarizer and a vortex waveplate [29,30]. The RPB then passes through another linear polarizer to produce the HG_{10} beam, and is further focused by a microscope objective (NA = 0.6) onto the sample structure. The scattered and reflected light from the structure is collected by the same objective, and the Fourier plane of the objective is imaged at a split detector through a beam splitter and a 4-f system. The intensity and phase pattern of the generated HG_{10} beam before the microscope objective are shown in Fig. 1(b), and the focused beam at the plane of the structure has been calculated by a three-dimensional Fourier transform method based on Debye-Wolf integral [31–33], with FWHM of the focus size is 1.15 um. As shown in Fig. 1(b), a zero-intensity singularity line appears in the middle of the pattern, with a π - phase jump between the two sides across the singularity. The black arrows in Fig. 1(b) indicates the direction of the polarization.

Figure 1(c) schematically shows the situation when the focused linear singularity is aligned along the edge of the step-shaped sample (named the parallel configuration), where the left side lobe of focused HG_{10} beam is projected onto the lower surface of step structure and the right one onto the upper surface. The incident HG_{10} beam can be freely rotated by changing the direction of linear polarizer 2, and therefore the angle between the singularity line and the edge of nanostructure is tunable. In addition to the parallel configuration, we also consider the other typical situation named perpendicular configuration, where the line singularity of HG_{10} beam is perpendicular to the edge of the structure, which can be achieved by rotating the polarizer 2 (or the sample) by 90° w.r.t. the parallel configuration. Note that these configurations can also be obtained by keeping the input beam fixed and rotating the sample laterally. The sensitivities of the two configurations due to the structural parameters are discussed in details in the following sections.

For numerical analysis of the scattered far field intensity of the structure, a 3-dimentional finite-different time-domain (FDTD) model is built. The HG_{10} illumination source is generated through a self-written script, and its singularity line is tunable and rotatable. In simulations, the computational convergence must be satisfied to keep the validity, and the simulation will

Optics EXPRESS

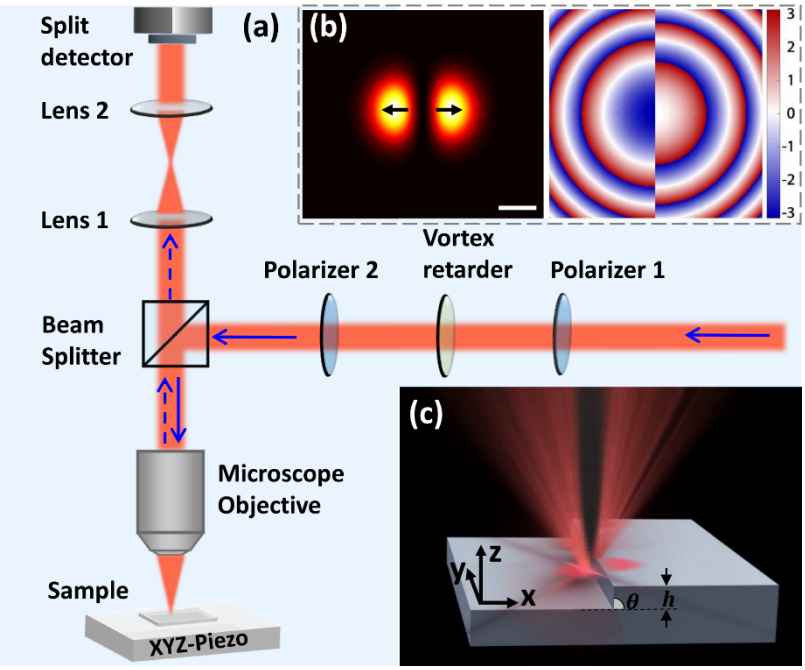

Fig. 1. (a) Scheme of the bimodal detection system based on a reflective coherent scatterometer illuminated by a singular beam. A collimated laser beam passes through two linear polarizers with a vortex retarder in between to generate the desired HG_{10} beam. This beam is then focused onto the sample by a microscope objective. The scattered and reflected light is collected by the same objective and finally analyzed by the split detector. (b) The intensity and phase distribution of the HG_{10} beam. The polarization is perpendicular to the singularity line as indicated by the black arrows. Scalebar is 500 nm. (c) 3D view of the interaction between HG_{10} beam and step-shaped silicon nanostructure.

complete successfully and shut off automatically when convergence criteria is satisfied. In the model, a fine computing grid will ensure the accuracy of the results, but meanwhile introduce additional computations to increase the run time. To trade off the run time and computational precision, the grid size in the step structure region, made of silicon (index of refraction n = 3.882 at 633 nm), is set as 2 nm in x-y plane and 5 nm in z-direction. A perfect matching layer (PML) boundary condition is employed for all simulations. For a high distinguish accuracy, a split-detector, aligned with its split line along the y direction, is implemented here by recording and integrating the signals on each half of the split detector separately.

3. Simulation results and discussion

In our previous works [34,35], we have focused on the SWA measurements with the precondition that the height of the step-shaped structure is already known. However, in a more general case, both parameters are not known, thus we need to figure out the effects of both parameters on the scattered far-field intensity. To reveal the effect of the height of structure, Fig. 2 presents the intensity profiles of the back-scattered field in the back focal plane of the objective at three different heights of 0 nm, 80 nm (≈ 1/8 λ), and 160 nm (≈ 1/4 λ). The SWA is set to be 90° in all cases. The upper row in Fig. 2 is measured in the parallel configuration for the incident beam as indicated in Fig. 1(c), and the lower row is measured in the perpendicular configuration. The bold solid white line in the figure corresponds to the edge of the step structure.

Optics EXPRESS

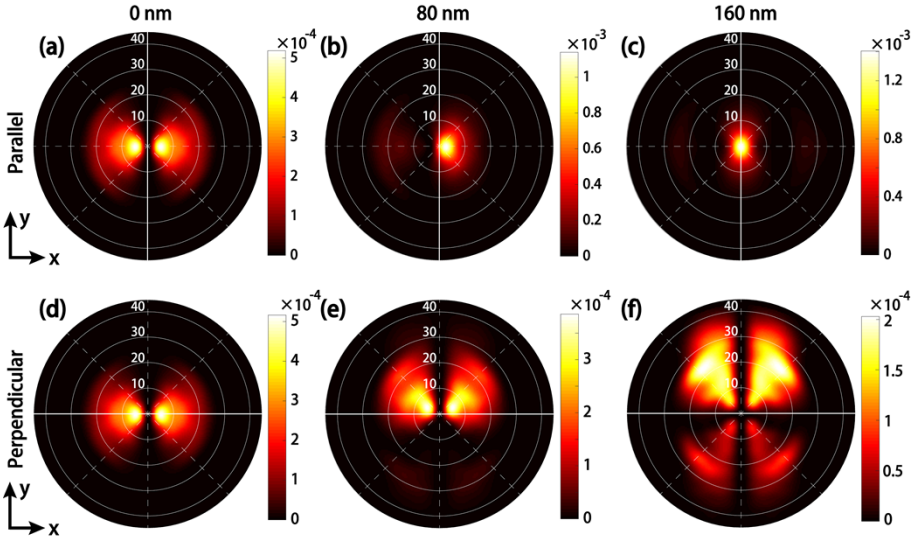

Fig. 2. The far-field intensity distributions at the back focal plane of the objective when a HG beam is focused on a step (silicon) with variable height and fixed SWA = 90 degrees. The upper (a-c) and lower (d-f) rows are simulated when the singularity line is parallel and perpendicular to the step (shown as a white line in the plots), respectively. The three columns correspond to three different structure heights: 0 nm, 80 nm, and 160 nm. The wavelength is 633 nm and the numerical aperture is 0.6.

As shown in Figs. 2(a) and 2(d) at the height of 0 nm, the scattered fields are nearly the same, which is just reflected by a flat surface and thus the profile is similar to the HG_{10} beam shown in Fig. 1(b). With an increased height of the step-structure, as shown from Fig. 2(a) to 2(c), the scattered intensity in the left hemisphere becomes weaker while the right lobe gradually moves to the center. In Fig. 2(c), the scattered field with a bright spot in the center is very similar to a Gaussian beam, mainly because the phase difference of reflected light introduced by the height of 160 nm is around π, which nicely compensates the inherent π - phase jump of HG_{10} beam as shown in Fig. 1(b). Similarly, for the perpendicular configuration in Fig. 2(d) to 2(f), the main lobes of the scattered field gradually move to the upper hemisphere, and another dark line is formed along the horizontal direction with the increase of height. As shown in Fig. 2(f), the horizontal dark line caused by the sample is perpendicular to the singularity line of HG_{10} beam, and divides the scattered field into four quadrants. Notably, the far-field intensity distribution of the scattering field strongly depends on the height of the step, hence providing an alternative approach for retrieving the value of the height of the structure.

To quantify the discernibility of the configuration, the scattered signal in the far-field is divided into the left/up and right/down halves for split detection, with the split line of the split detector parallel to the step structure in accordance with Fig. 2. The split detection signal is obtained by integrating the intensity on both halves of the split detector and subtracting them. The signal is then normalized by the total intensity (i.e., the sum of the intensities of both halves of the split detector). Several Height-SWA combinations are investigated by sweeping the height from 0 nm to 400 nm and SWA from 80° to 90°, in parallel and perpendicular configuration, as shown in Figs. 3(a) and 3(b), respectively. The results indicate that height of the structure has a dominated influence the value of the split detection signal, while the SWA makes a minor impact.

For further confirmation of the different roles of the two parameters, a more accurate sweeping is carried out for both configurations as depicted in Fig. 3(c). Here, the value of height is swept

Optics EXPRESS

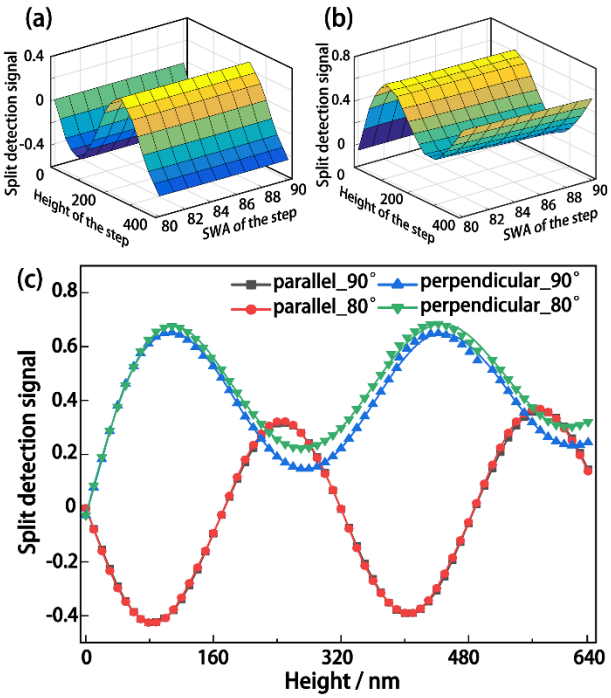

Fig. 3. The split detection analysis for different Height-SWA combinations. 3-D view of the split detection signals by sweeping both the height and the SWA of the structure in parallel (a) and perpendicular (b) configuration, respectively. Both the scale and color represent the value of split detection signal. (c) Larger region and higher precision height sweeping with SWAs of 80° and 90° in both configurations. Note that the black and red curves almost overlap everywhere.

from 0 nm to 630 nm in both configurations, and two typical SWAs (80° and 90°) are selected for comparison. Black and red curves in the parallel configuration highly coincided in the entire range, proving that the effect of SWAs is negligible in this case. In this configuration, the changes in the split detector value are more sensitive for changes in the height of the structure, so the split detection signal can be used for accurate determination of the height.

On the contrary, the blue and green curves (corresponding to two different SWA in the perpendicular configuration) are highly coincided when the height is below 100 nm, but show differences with increasing height. The difference is much bigger around the height of 280 nm and 590 nm, corresponding to the valley of the curves. Compared to the parallel case, the perpendicular configuration shows a better performance on the discrimination of SWAs. Although in Fig. 3(c) the effect of height is quasi-periodic in all curves, accurate height value of the structure can still be determined based on the combined results of the two configurations.

With calibrated heights of the nanostructure, Fig. 4 shows quantitative comparisons of the split detect signals for five SWAs at different heights. The sample is fixed and the singularity line of the incident beam is rotated from 0° to 180°, i.e., from the parallel to the perpendicular configuration and finally back to the parallel situation. Whereafter, the split detection value is plotted as a function of the rotation angle, and the curves for five different SWAs are self-normalized by the maximum value. The difference within each set of curves in Fig. 4(a) gives the index to evaluate the distinguish capability of the singular beam. It is clear that the signals for SWAs of $\theta = 80°$ and 90° are the top curve and the bottom curve, respectively, and the peaks of different values of

Optics EXPRESS

the detected signals for various SWAs are obtained at the perpendicular mode when rotating the singularity direction of the singular beam. To clearly compare the distinguish capability at the perpendicular mode, we plot in Fig. 4(b) the normalized split detection signal as a function of the SWA for different heights. For a certain height, the difference value compared to the reference point (SWA = 80°) shows a monotone variation, and for each SWA, a unique split detection signal is obtained. Consequently, the perpendicular mode is capable to determine the SWAs. The slope of the curve can be used to quantify the distinguish capability. One notices also that it is easier to determine the SWA when the step is not very shallow.

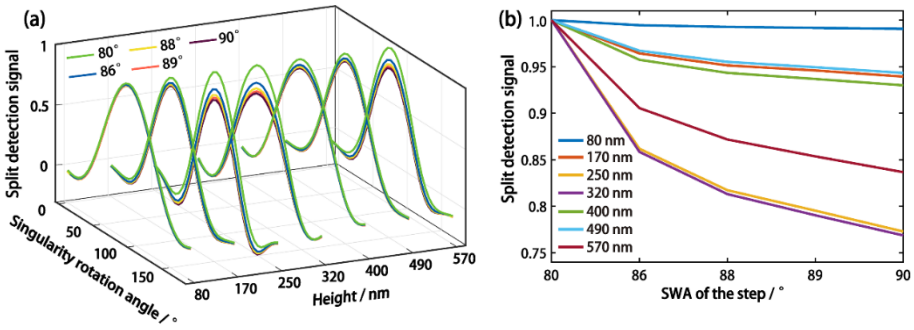

Fig. 4. (a) The split detection signals as a function of the rotation angle for five SWAs and seven different heights. The signal is generated by rotating the singularity from 0° to 180°, of which the 0° and 180° rotation angles correspond to the parallel configuration, and the center rotation angle (90°) corresponds to the perpendicular one. (b) The normalized split detection signal in perpendicular mode as a function of the SWA for different structure heights.

From the results of the perpendicular case in Fig. 3(c), one can achieve a comprehensive understanding on the dependence of the signal as a function of the height variations. The differences between curves at 80° and 90° are more pronounced within a certain height interval (close to integer multiples of the half-wavelength), as there exists a π-phase difference on both sides of the singularity line. This reveals that the SWAs can be better distinguished in these height intervals than others. It should be noted that the lateral shadow of the step-structure with low height is ultra-small. For instance, the shadow difference between 89° and 90° is only 1.4 nm for the height of 80 nm, which is an extremely tiny value to be distinguished. Consequently, the five curves are highly coincident at the height h = 80 nm, indicating that it is still a challenge for the proposed method to distinguish the SWAs in the case of shallow steps.

Based on the above analysis, the height can be calibrated with high accuracy without the influence of SWA in the parallel configuration. By rotating the singularity line in a suitable height interval, our method can be successfully used to distinguish steep SWAs. Ultimately, with a combination of the above two processes, e.g., focusing the singularity line along the step-structure and rotating the singularity line, both the height and SWA of the structure can be retrieved simultaneously. Moreover, the mechanical vibrations can be effectively evaded by just rotating the singularity line of the incident beam. The rotation allows disambiguation and decoupling of the experimental signal from the effect of experimental noise by allowing for multiple measurements, which helps to improve the measurement accuracy. This is a great improvement compared with previous works [34,35].

For real-life samples, many of them often include steps that are made from a different material on and off the step. Due to the different scattering and reflection efficiency of the two materials, the intensity and phase shift between the two regions will be changed and will affect the intensity contrast. Moreover, most functional structures are constituted by series of monomer units, where

Optics EXPRESS

the boundary conditions are periodic. For this case, the numerical effort will be ultra-high, simple surrogate models, e.g., polynomial chaos approach [36], will open a new window for the CFS modelling. These are very valuable and meaningful subjects for accurate nanoscale detection in practical applications. We will focus on these topics and carry out the retrieval research in our following works.

4. Conclusion

In conclusion, we employed a HG10 mode singular beam to combine with the conventional CFS system to retrieve the geometrical parameters of structures that are commonly used in the semiconductor industry. For simplicity but without loss of generality, a 3-D step-shaped structure with an invariant y-axis is selected as the sample. Using our method, it is possible to determine both the height and the SWA of the structure simultaneously by rotating the singularity direction of HG10 beam and measuring the far field with a split detector. This provides a much simpler and more robust approach than the raster scanning method in conventional CFS. When the singularity is parallel to the invariant axis of the sample, the height can be accurately detected regardless of the influence of SWA. By rotating the angle of the singularity line of the singular beam w.r.t. the direction of the edge of the structure, one can retrieve the SWA with high accuracy in a suitable height interval. The proposed method can work under wide conditions, being not limited to the step-structures. The same applies to more varied materials, structures, wavelengths, etc., and these will be further discussed in the following research. Given that the height interval where the sensitivity is high depends on the wavelength, one can tailor the sensitivity region by varying the wavelength of the illumination. This work will open up new opportunities for precision measurements in semiconductor industries.

Funding. Guangdong Major Project of Basic and Applied Basic Research (2020B030103000); National Natural Science Foundation of China (61935013, 61975128, 62175157); Leading Talents of Guangdong Province Program (00201505); Natural Science Foundation of Guangdong Province (2019TQ05X750); Shenzhen Peacock Plan (KQTD20170330110444030); Science and Technology Innovation Commission of Shenzhen (RCJC20210609103232046, ZDSYS201703031605029).

Disclosures. The authors declare no conflicts of interest.

Data availability. Data underlying the results presented in this paper are not publicly available at this time but may be obtained from the authors upon reasonable request.

References

1. H. Wang and M. L. Gee, "AFM lateral force calibration for an integrated probe using a calibration grating," Ultramicroscopy **136**, 193–200 (2014).
2. N. Jalili and K. Laxminarayana, "A review of atomic force microscopy imaging systems: application to molecular metrology and biological sciences," Mechatronics **14**(8), 907–945 (2004).
3. O. Jusko, X. Zhao, H. Wolff, and G. Wilkening, "Design and three dimensional calibration of a measuring scanning tunneling microscope for metrological applications," Rev. Sci. Instrum. **65**(8), 2514–2518 (1994).
4. G. Dai, M. Heidelmann, C. Kübel, R. Prang, J. Fluegge, and H. Bosse, "Reference nano-dimensional metrology by scanning transmission electron microscopy," Meas. Sci. Technol. **24**(8) (2013).
5. C. G. Frase, E. Buhr, and K. Dirscherl, "CD characterization of nanostructures in SEM metrology," Meas. Sci. Technol. **18**(2), 510–519 (2007).
6. C. Raymond, "Overview of Scatterometry Applications In High Volume Silicon Manufacturing," In *AIP Conference Proceedings*, 2005; pp 394–402.
7. M. H. Madsen and P.-E. Hansen, "Scatterometry—fast and robust measurements of nano-textured surfaces. Surface Topography: Metrology and Properties," 2016, 4 (2).
8. H. Gross, S. Heidenreich, M. A. Henn, G. Dai, F. Scholze, and M. Bär, "Modelling line edge roughness in periodic line-space structures by Fourier optics to improve scatterometry," JEOS:RP **9**, 14003 (2014).
9. P. Petrik, N. Kumar, M. Fried, B. Fodor, G. Juhasz, S. F. Pereira, S. Burger, and H. P. Urbach, "Fourier ellipsometry – an ellipsometric approach to Fourier scatterometry," JEOS:RP **10**, 15002 (2015).
10. V. Ferreras Paz, S. Peterhänsel, K. Frenner, and W. Osten, "Solving the inverse grating problem by white light interference Fourier scatterometry," Light: Sci. Appl. **1**(11), e36 (2012).
11. E. Gawhary, O. Kumar, N. Pereira, S. F. Coene, and W. M. J. P. H. Urbach, "Performance analysis of coherent optical scatterometry," Appl. Phys. B **105**(4), 775–781 (2011).

Optics EXPRESS

12. N. Kumar, P. Petrik, G. K. Ramanandan, O. El Gawhary, S. Roy, S. F. Pereira, W. M. Coene, and H. P. Urbach, "Reconstruction of sub-wavelength features and nano-positioning of gratings using coherent Fourier scatterometry," Opt. Express **22**(20), 24678 (2014).
13. B. Wang, M. Tanksalvala, Z. Zhang, Y. Esashi, N. W. Jenkins, M. M. Murnane, H. C. Kapteyn, and C. T. Liao, "Coherent Fourier scatterometry using orbital angular momentum beams for defect detection," Opt. Express **29**(3), 3342–3358 (2021).
14. D. Kolenov, I. E. Zadeh, R. C. Horsten, and S. F. Pereira, "Direct detection of polystyrene equivalent nanoparticles with a diameter of 21 nm (approximately lambda/19) using coherent Fourier scatterometry," Opt. Express **29**(11), 16487–16505 (2021).
15. S. Roy, A. C. Assafrao, S. F. Pereira, and H. P. Urbach, "Coherent Fourier scatterometry for detection of nanometer-sized particles on a planar substrate surface," Opt. Express **22**(11), 13250 (2014).
16. A. Forbes, M. de Oliveira, and M. R. Dennis, "Structured light," Nat. Photonics **15**(4), 253–262 (2021).
17. Y. Yang, Y.-X. Ren, M. Chen, Y. Arita, and C. Rosales-Guzmán, "Optical trapping with structured light: a review," Adv. Photonics **3**(03), 034001 (2021).
18. H. Rubinsztein-Dunlop, A. Forbes, M. V. Berry, M. R. Dennis, D. L. Andrews, M. Mansuripur, C. Denz, C. Alpmann, P. Banzer, T. Bauer, E. Karimi, L. Marrucci, M. Padgett, M. Ritsch-Marte, N. M. Litchinitser, N. P. Bigelow, C. Rosales-Guzmán, A. Belmonte, J. P. Torres, T. W. Neely, M. Baker, R. Gordon, A. B. Stilgoe, J. Romero, A. G. White, R. Fickler, A. E. Willner, G. Xie, B. McMorran, and A. M. Weiner, "Roadmap on structured light," J. Opt. **19**(1), 013001 (2017).
19. M. R. Dennis, K. O'Holleran, and M. J. Padgett, "Chapter 5 Singular Optics: Optical Vortices and Polarization Singularities," 2009; pp 293–363.
20. D. Mao, Y. Zheng, C. Zeng, H. Lu, C. Wang, H. Zhang, W. Zhang, T. Mei, and J. Zhao, "Generation of polarization and phase singular beams in fibers and fiber lasers," Advanced Photonics 2021, 3 (01).
21. B. N. A. Spektor and J. Shamir, "Singular beam microscopy," Appl. Opt. **47**(4), A78–A87 (2008).
22. G. H. Y. A. N. I. Zheludev, "Detecting nanometric displacements with optical ruler metrology," Science **364**(6442), 771–775 (2019).
23. W. Wang, T. Y. Reika Ishijima, A. Wada, Y. Miyamoto, and M. Takeda, "Optical vortex metrology for nanometric speckle displacement measurement," Opt. Express **14**(1), 120–127 (2006).
24. Z. Xi, L. Wei, A. J. Adam, H. P. Urbach, and L. Du, "Accurate Feeding of Nanoantenna by Singular Optics for Nanoscale Translational and Rotational Displacement Sensing," Phys. Rev. Lett. **117**(11), 113903 (2016).
25. A. K. Asundi, M. L. Gödecke, W. Osten, K. Frenner, D. Buchta, and S Peterhänsel, "Detection of grating asymmetries by phase-structured illumination," In *Fifth International Conference on Optical and Photonics Engineering*, 2017.
26. A. Faridian, V. F. Paz, K. Frenner, G. Pedrini, A. D. Boef, and W. Osten, "Phase-sensitive structured illumination to detect nanosized asymmetries in silicon trenches," J. Micro/Nanolithogr., MEMS, MOEMS **14**(2), 021104 (2015).
27. E. S. B. Hemo and J. Shamir, "Scattering of singular beams by subwavelength objects," Appl. Opt. **50**(1), 33–42 (2011).
28. J. Shamir, "Singular beams in metrology and nanotechnology," Opt. Eng. **51**(7), 073605 (2012).
29. X. Dou, A. Yang, C. Min, L. Du, Y. Zhang, X. Weng, and X. Yuan, "Polarization-controlled gap-mode surfaceenhanced Raman scattering with a single nanoparticle," J. Phys. D: Appl. Phys. **50**(25), 255302 (2017).
30. T. Zang, H. Zang, Z. Xi, J. Du, H. Wang, Y. Lu, and P. Wang, "Asymmetric Excitation of Surface Plasmon Polaritons via Paired Slot Antennas for Angstrom Displacement Sensing," Phys. Rev. Lett. **124**(24), 243901 (2020).
31. J. Lin, O. G. R.-H.F. Kenny, D. Lara, and J. C. Dainty, "Fast vectorial calculation of the volumetric focused field distribution by using a threedimensional Fourier transform," Opt. Express **20**(2), 1060–1069 (2012).
32. M. Leutenegger, R. R. Rainer A, and T. L. Leitgeb, "Fast focus field calculations," Opt. Express **14**(23), 11277–11291 (2006).
33. B. R. A. E Wolf, "Electromagnetic diffraction in optical systems," II. Structure of the image field in an aplanatic system. Proceedings of the Royal Society of London. Series A. Mathematical and Physical Sciences **253**, 358–379 (1959).
34. X. Dou, S. F. Pereira, C. Min, Y. Zhang, P. Meng, H. P. Urbach, and X. Yuan, "Determination of steep sidewall angle using polarization-sensitive asymmetric scattering," Meas. Sci. Technol. **32**(8), 085201 (2021).
35. L. Cisotto, S. F. Pereira, and H. P. Urbach, "Analytical calculation on the determination of steep side wall angles from far field measurements," J. Opt. **20**(6), 065601 (2018).
36. M. Tootkaboni, A. Asadpoure, and J. K. Guest, "Topology optimization of continuum structures under uncertainty–a polynomial chaos approach," Computer Methods in Applied Mechanics and Engineering **201-204**, 263–275 (2012).